DOI: 10.1002/ ((please add manuscript number))

Article type: Full Paper

Characterization of the Valence and Conduction Band Levels of n=1 Two-Dimensional Perovskites: A Combined Experimental and Theoretical Investigation

*Scott Silver, Jun Yin, Hong Li, Jean-Luc Brédas, Antoine Kahn**

S. Silver, Prof. A. Kahn

Department of Electrical Engineering, Princeton University, Princeton, New Jersey 08544, United States

Email: kahn@princeton.edu

Dr. J. Yin

Division of Physical Sciences and Engineering, King Abdullah University of Science and Technology (KAUST), Thuwal 23955-6900, Saudi Arabia

Dr. H. Li, Prof. J-L. Brédas

School of Chemistry and Biochemistry and Center for Organic Photonics and Electronics, Georgia Institute of Technology, Atlanta, Georgia, 30332-0400, USA.

Keywords: perovskites, two-dimensional materials, quantum wells, photoelectron spectroscopy, DFT calculations

This study presents a combined experimental and theoretical study of the electronic structure of two two-dimensional (2D) metal halide perovskite films. Ultraviolet and inverse

photoemission spectroscopies (UPS, IPES) are performed on solution-processed thin films of the *n*=1 layered perovskite butylammonium lead iodide and bromide, BA_2PbI_4 and BA_2PbBr_4, characterized by optical absorption and X-ray diffraction, to determine their valence and conduction band densities of states, transport gaps, and exciton binding energies. The electron spectroscopy results are compared with the densities of states determined by density functional theory calculations. The remarkable agreement between experiment and calculation enables a detailed identification and analysis of the organic and inorganic contributions to the valence and conduction bands of these two hybrid perovskites. The electron affinity and ionization energies are found to be 3.1 and 5.8 eV for BA_2PbI_4, and 3.1 and 6.5 eV for BA_2PbBr_4. The exciton binding energies are estimated to be 260 meV and 300 meV for the two materials, respectively. The 2D lead iodide and bromide perovskites exhibit significantly less band dispersion and a larger density of states at the band edges than the 3D analogs. The effects of using various organic ligands are also discussed.

1. Introduction

Metal halide perovskites (MHPs) of the type AMX_3 (A: organic cation; B: metal cation; and X: halide anion) are potential major players in the future of solar cells and light-emitting devices.[1–3] In the on-going research effort to optimize these MHP materials and their device applications, electronic structure is a valued piece of information, particularly the energy and density of states (DOS) near the conduction and valence band edges, which are central to all optoelectronic properties and charge carrier transport processes. Several electron spectroscopy studies have been devoted to MHP materials,[4–8] however, achieving accurate descriptions of band edges and associated parameters, such as electron affinity (EA) and ionization energy (IE), on bulk MHPs like methylammonium and cesium lead halides has

remained difficult and sometimes inconsistent. Beyond standard issues of reproducibility due to sample processing and composition, one specific difficulty is the unusually low DOS at the band edges, particularly at the valence band maximum (VBM) of these lead compounds. This issue has been pointed out in theoretical investigations by Kawai *et al.*,[9] as well as in a combined experimental-theoretical investigation by Endres *et al.*[10] Low DOS at the VBM has been proposed to play a significant role in carrier transport and absorption properties of the material. It has also been tentatively linked to carrier dynamics and slow hot-hole cooling at high excitation densities, which provides the option for hot carrier extraction.[9,11] Additionally, it has been suggested that it could be a contributing factor to the high open-circuit voltage (V_{OC}) generally obtained from MHP solar cells.[12]

Air, moisture, and light vulnerabilities in the standard bulk MHPs have led to considerable interest in the seemingly more stable homologous two-dimensional (2D) layered MHPs (LMHPs), of the type $A'_2A_{n-1}M_nX_{3n+1}$, where *n* is the number of inorganic repeat layers sandwiched between the organic ligands[13–16]. It is important to note, that these LMHPs no longer exhibit the "perovskite" structure, and are more accurately described as Ruddlesden-Popper phases, still, they frequently bear the name "perovskites" in the literature due to their similarities to MHPs in terms of constituents, properties, processing and applications. These LMHPs in various forms have found applications as active layers for light-emitting diode and solar cell devices,[3,17–21] as well as capping layers for bulk MHP cells, and also have the potential to serve in tandem solar cells. Yet, the electronic transport energy levels and fundamental gap of these materials are poorly understood due to the lack of characterization of the DOS near the valence band edge and of the exciton binding energy, which brings an additional layer of complication as the exciton binding energy in the 2D

materials has been up for discussion. Initial calculations for n=1 yielded values as high as 390 meV in 2D lead iodide perovskites,[22] in accord with experimental estimations of about 360 meV at cryogenic temperatures, where multiple excitonic levels are resolvable.[23] However, 2D lead iodide perovskites undergo a phase change below room temperature[24] and screening by the organic components has been shown to reduce the exciton binding energy considerably at higher temperatures, a feature not previously accounted for in the calculations.[25]

To gain insight into the electronic structure and energetics of LMHPs, we perform here a combined experimental and theoretical investigation of 2D n=1 butylammonium lead iodide (BA_2PbI_4) and bromide (BA_2PbBr_4) perovskites. We compare the transport gap determined by ultra-violet and inverse photoemission spectroscopy (UPS, IPES) at room temperature with the optical gap, and deduce a room temperature value for the exciton binding energy in these two materials. We also provide a comparison of the DOS at the band edges with those of the three-dimensional bulk analogs.

2. Results and Discussion

The 2D crystal structure of the BA_2PbI_4 and BA_2PbBr_4 films was confirmed with X-Ray Diffraction (XRD) and optical absorption measurements. From the XRD spectra of **Figure 1**a, the (002) d-spacing is determined to be 1.383 nm and 1.379 nm for BA_2PbI_4 and BA_2PbBr_4, respectively, which is consistent with previous results.[26] No features hinting at any other structure than the n=1 2D structure can be observed. The absorption spectra (Figure 1b) show clear exciton peaks for both films, followed by distinct onsets of interband absorption. AFM micrographs show pronounced grain structures for both compounds,

pictured for a BA_2PbI_4 film in Figure 1b. The average grain size is 500 nm and individual grains show smooth surfaces with RMS roughness of 4 nm (see Figures 1c and 1d).

The BA_2PbI_4 and BA_2PbBr_4 valence and conduction band spectra measured via UPS (He-II) and IPES are plotted in **Figure 2** and compared to the DFT densities of states calculated at the HSE+SOC level. In accord with standard procedures,[27] the calculated DOS of the valence band is shifted and stretched (10%) to best match the valence features determined via He-II UPS. The calculated DOS of the conduction band was stretched by the same amount, but shifted independently to line up with the experimental conduction band edge determined by IPES. The experiment-theory comparison is shown in Figures 2a and 2c with the various contributions from each orbital to the calculated DOS shown in Figures 2b and 2d for the iodide and bromide compound, respectively. The excellent agreement between experiment and theoretical results enables a precise alignment between the spectra. Accordingly, the edges of the DFT calculated valence bands are found at 2.0 eV and 3.0 eV below the Fermi level (E_F) for BA_2PbI_4, and BA_2PbBr_4, respectively. The top of the experimental valence band exhibits a larger peak in the BA_2PbBr_4 case than in the BA_2PbI_4 case, owing to the larger photoionization cross-section for the Br 4*p* orbital (0.97) relative to the I 5*p* orbital (0.78) at He-II photon energy. Similarly, the large experimental intensity of the butylammonium states is consistent with the photoionization cross-section of the C 2*p* orbital (1.88).[28] The large contribution of the organic ligand to the valence and conduction band spectra is also consistent with the predominance of the organic part relative to the inorganic framework (Pb and halides) in such *n*=1 2D structures.

The UPS He-I spectra of the valence band edge of both films are compared to the DFT results in **Figure 3**. The agreement between spectral line shapes is excellent, especially for

the Br compound. Having precisely aligned experimental and simulated spectra, we use the calculated valence band edge of each compound as well as the corresponding UPS-determined work function (3.8 eV for BA_2PbI_4 and 3.5 eV for BA_2PbBr_4) to determine the ionization energy (IE) and electron affinity (EA) of the films. For BA_2PbI_4, we find IE = 5.8 eV and EA = 3.1 eV, whereas the values are IE = 6.5 eV and EA = 3.1 eV for BA_2PbBr_4.

In contrast to 3D perovskites, which exhibit strong dispersion at the top of the valence band[22,29] and thus an unusually small DOS near the valence band edge that requires careful consideration on a logarithmic scale when measured in UPS,[10] the DOS leading up to the valence band edge of the 2D compounds is larger and can be resolved on a standard linear scale plot. This owes in part to the anisotropic band dispersion at the top of the valence band, which displays a totally flat (non-dispersive) part along the Γ-Z direction (perpendicular to the 2D plane) coinciding with a very dispersive part along the Γ-X direction (in the 2D plane) **(Figure 4)**. The non-dispersive part is reflective of the lack of wavefunction overlap between adjacent inorganic lead-halide layers separated by the organic ligands. In that regard, quantum confinement, in addition to increasing the band gap of the 2D material relative to its 3D analog, also leads to an abrupt rise in the DOS near the valence band edge.[30] A direct comparison of the valence band edge of 2D and 3D perovskites is shown in the Supporting Information (Figure S2). The calculated electron and hole effective masses along the Γ-X direction representing in-plane transport, shown in Table 1, are on the order of 0.1 m_0 and smaller than the masses previously determined experimentally[31,32] and theoretically[33,34] for 3D MHPs, but agree well with previous predictions for similar 2D MHPs.[35] The effective mass of holes was calculated to be larger than that of electrons consistent with earlier calculation done for 3D MHPs.[36] This contrasts with previous findings that quantum

confinement increased the in-plane effective mass relative to the bulk in CdSe nanoplatelets.[37] Finally, we note that the effects of spin-orbit coupling on the band structure (Figure 4) and effective masses (Table 1) are more significant in BA_2PbI_4 than in BA_2PbBr_4 due to the heavier I ions.

We now turn to the exciton binding energies (E_B) and other properties of these n=1 systems in the context of quantum confinement. The optical gaps for these materials are found to be 2.38 eV for BA_2PbI_4 and 3.04 eV for BA_2PbBr_4 based on a linear extrapolation of the low energy edge of the exciton peak on a Tauc plot (see Figure S3 in the Supporting Information). Similarly, the onset of the interband absorption can be estimated as 2.64 eV for BA_2PbI_4 and 3.34 eV for BA_2PbBr_4. From these onsets, we can deduce the exciton binding energies (E_B) of BA_2PbI_4 and BA_2PbBr_4 to be 260 meV and 300 meV, respectively, values that are smaller relative to those previously determined from low-temperature measurements.[23,38,39] However, using the same linear approximation of the interband absorption onset, other studies have found varying results for the same materials,[40–42] pointing to the limits of this method. Alternatively, we can estimate E_B using the single particle gap determined via the combination of UPS and IPES, and the optical gap determined by the onset of optical absorption. The optical gap reflects the minimum energy required to form a bound exciton in the material, whereas the band gap determined by UPS and IPES represents the energy difference between uncorrelated free electron and hole. The difference between these two values is E_B, which, according to our data, is 300 meV for BA_2PbI_4 and and 400 meV for BA_2PbBr_4. E_B is expectedly larger in BA_2PbBr_4 because of the smaller polarizability of the Br ion relative to the I ion in the inorganic framework of the lattice. These values are more than one order of magnitude larger than binding energies in 3D

halide perovskites (tens of meV).[31,43] The difference in E_B between the bulk perovskite and the homologous 2D structure can be attributed to the effect of quantum confinement, the dielectric constant, and the excitonic effective mass. Indeed, E_B is increased, up to a factor of four, by quantum confinement in an ideal 2D system.[44] Furthermore, E_B is typically inversely proportional to the square of the dielectric constant of the material,[44] which in the present case is significantly lowered with respect to the 3D analog by the predominance of the butylammonium organic ligands in the volume of the 2D n=1 material. On the other hand, E_B is also proportional to the reduced effective mass defined as:

$$\frac{1}{m^*} = \frac{1}{m_n^*} + \frac{1}{m_p^*} \#(1)$$

where m_n^* and m_p^* are the electron and hole effective masses[45], respectively. According to the DFT calculations shown in Table 1, m^* ($0.039m_0$ in BA_2PbI_4 along the Γ-X direction) is only a fraction of what has been determined experimentally for bulk $MAPbI_3$ ($0.10m_0$)[31]. The experimental results described above suggest that this effect is largely negated by the quantum and dielectric confinements, which tend to increase E_B.

Using our theoretical and experimental data in combination with the electron energy levels determined in corresponding 3D MHPs, we can estimate the depth of both the electron and hole quantum wells in the LMHPs, as shown in **Figure 5**. We consider that the bottom of the conduction band and top of the valence band in the quantum well (E_C and E_V) in the 2D n=1 compounds correspond to the energy of the conduction band and valence band edges, respectively, of the $n=\infty$ (3D) compound. We use the ionization energy and electron affinity determined by Endres *et al*.[10] for 3D $MAPbI_3$ (IE = 5.2 eV, EA = 3.6 eV) and $MAPbBr_3$ (IE = 6.0 eV, EA = 3.7 eV) to define the energy position of E_C and E_V (Figure 5). The finite

heights of the conduction and valence band wells are defined by the position of the lowest unoccupied and highest occupied butylammonium states, respectively, determined from the alignment between DFT calculation and experiment for BA_2PbI_4 (6.5 eV, below vacuum level for the filled states and 1.5 eV for the empty states) and BA_2PbBr_4 (7.6 eV and 1.0 eV) (Figure 2). Electrons or holes with energy sufficient to access these ligand-associated states are free to move across the 2D layers and are, in principle, not confined to the quantum well. The experimental ground-state energy levels for the electron and hole (Figure 5) correspond to the bottom of the conduction band and top of the valence band measured by IPES and UPS, respectively, for the two 2D n=1 compounds (Figure 2).

To interpret the results, we can apply the Kronig-Penney model[46] adapted for superlattices [47–49] to the multiple quantum wells formed in these materials as a means of approximating the energy levels. The heights of the potential wells determined above in combination with the effective masses of the bulk perovskite materials taken from the literature[31,50], and the well and barrier widths determined by XRD were input into the Kronig-Penney model to estimate the ground state energy of the electron and hole in the quantum wells, or IE and EA in the n=1 materials (see Supporting Information). The effective mass in the butylammonium layer is empirically taken to be 1.0 m_0 as on-going work on these 2D compounds show that this value can also be used to accurately model experimental data in n=2, 3, and 4 materials as well. This value, in the context of the Kronig-Penney model applied to 2D perovskites, describes the electronic transport in the direction perpendicular to the QW, along the butylammonium chain. The relatively low effective mass of 1.0 m_0 is therefore a reasonable parameter. Furthermore, The resulting values of IE and EA line up remarkably well with our experimentally determined values, as shown in Figure 5. By

changing the width of the barrier layer in the model, the band gap remains unchanged, indicating that there is no significant electronic communication between the inorganic layers, which is consistent with the perfectly flat bands in the Γ-Z direction of the DFT calculated band structure (Figure 4).

The properties of the organic barrier layer will have multiple effects on the transport gap of the 2D compound. First, the organic contribution to the valence and conduction bands will affect the depth of their respective quantum wells. Second, the width and nature of the organic layer will influence the electronic communication between the inorganic layers. A careful choice of the organic ligand should therefore enable tuning of the electron affinity and ionization energy for optimizing interfaces in devices utilizing LMHPs.

3. Conclusions

In conclusion, the UPS/IPES experimental data of the DOS of two LMHPs, BA_2PbI_4 and BA_2PbBr_4, in combination with DFT calculations allow us to identify the organic and inorganic contributions to the DOS and determine values for the electronic transport levels, band gap, and exciton binding energy at room temperature. We show that the larger DOS of these 2D materials near the band edges, because of their quantum confinement, contrasts with the high dispersion previously observed in their 3D equivalents and therefore are not expected to exhibit the effects associated with the low DOS in 3D perovskites. This is essential in designing efficient interfaces utilizing two-dimensional perovskites alone or as part of a tandem perovskite solar cell.

4. Experimental Section

4.1 Experimental Methods

Thin films of BA_2PbI_4 were prepared by mixing stoichiometric amounts of PbI_2 (Alfa Aesar) and BAI (made from equimolar amounts of butylamine and HI, Sigma Aldrich) in DMF in a nitrogen atmosphere to make a 0.5 M solution. The solution was heated to 50 °C for 30 minutes, until it was fully converted to a yellow solution. It was then spin-coated for 35 seconds at a spin speed of 5600 RPM and an acceleration of 5600 RPM/s, creating transparent yellow films, onto cleaned glass slides for absorption, atomic force microscopy (AFM) and X-ray diffraction (XRD) measurements, and on ITO/glass for UPS, IPES and X-ray photoemission spectroscopy (XPS) measurements. Visibly smooth films were produced without the use of an antisolvent. The films were then annealed for 30 minutes at 50 °C. A very similar procedure was followed for BA_2PbBr_4, using $PbBr_2$ (Alfa Aesar) and BABr (made from equimolar amounts of butylamine and HBr, Sigma Aldrich) in DMF. The solution, heated to 50 °C for 30 minutes, was colorless and, when spin-coated on glass or ITO, produced transparent colorless films. Again, smooth films were produced without the use of an antisolvent. The films were then also annealed for 30 minutes at 50 °C. The thickness of all the films ranged between 150 and 200 nm as determined using AFM, which is thick enough to assure there is no probing of the substrate, and thin enough to prevent sample charging during electron-spectroscopy measurements. All samples were kept in the dark in a nitrogen atmosphere until they were measured.

XRD was performed using a Bruker D8 Discover X-Ray Diffractometer in ambient conditions on 200 nm thick samples deposited on glass. UV-Vis absorption measurements were taken on the perovskite films spun onto glass slides using a Cary 5000 Spectrometer under ambient conditions at room temperature.

UPS and IPES experiments were performed in ultra-high vacuum at room temperature on 1-cm^2 samples. The samples were transferred directly from a nitrogen atmosphere to vacuum without ambient exposure. UPS was performed with He-I photons (21.22 eV) to probe the valence band edge as well as He-II photons (40.81 eV) to probe deeper into the valence band. Electrons were collected with a double-pass cylindrical mirror analyzer, with a resolution of 150 meV. IPES was performed in the isochromat mode, with electron energies of 5-15 eV over several spots on the sample to minimize sample damage due to the beam. The overall resolution of the IPES measurements was 450 meV.[51]

4.2 Computational Methods

Density functional theory (DFT) calculations were performed to further understand the experimental UPS and IPES results for BA_2PbI_4 and BA_2PbBr_4. The calculations were carried out at the generalized gradient approximation (GGA)/Perdew-Burke-Ernzerhof (PBE) level using the projector-augmented wave (PAW) method as implemented in the VASP code.[52,53] Starting from the experimental orthorhombic phase (space group: PBCA) and lattice parameters of BA_2PbI_4 (a = 8.863 Å, b = 8.682 Å, and c = 27.570 Å)[35] and BA_2PbBr_4 (a = 8.253 Å, b = 8.138 Å, and c = 27.403 Å)[54] at room temperature, the crystal structures were further optimized by relaxing both cell parameters and atomic coordinates until the total force on each atom was < 0.01 eV/$Å^{-1}$. The plane-wave cutoff energy was set to 500 eV and a Γ-centered 4×4×1 K-mesh in the Brillouin zone was employed for both BA_2PbI_4 and BA_2PbBr_4. The electronic bands and effective mass were also calculated at the GGA/PBE level without and with spin-orbit coupling (SOC) effects. The Heyd-Scuseria-Ernzerhof hybrid functional (HSE06) with SOC was then used to calculate the density of states (DOS) with a Gaussian smearing value of 0.3 eV. In addition, to closely examine the nature of the

band edge states, a much smaller Gaussian smearing of 0.05 eV was also adopted in the PDOS calculations; the results are given in the Supporting Information (Figure S1).

Supporting Information

Supporting information is available from the Wiley Online Library or from the author.

Acknowledgements

Work at Princeton was supported in part by a grant from the US-Israel Binational Science Foundation (Grant # 2014357) and by a grant from the Princeton Environmental Institute and Andlinger Center. Work at the Georgia Institute of Technology is supported in part by the Georgia Research Alliance and ONR under Award No. N00014-17-1-2208. Work at King Abdullah University of Science and Technology is supported by KAUST Supercomputing Laboratory. Fruitful discussions with Prof. Omer Yaffe are gratefully acknowledged.

Received: ((will be filled in by the editorial staff))
Revised: ((will be filled in by the editorial staff))
Published online: ((will be filled in by the editorial staff))

References

[1] National Renewable Energy Laboratory, *NREL Efficiency Chart*, **2017**.

[2] H. Cho, S.-H. Jeong, M.-H. Park, Y.-H. Kim, C. Wolf, C.-L. Lee, J. H. Heo, A. Sadhanala, N. Myoung, S. Yoo, S. H. Im, R. H. Friend, T.-W. Lee, *Science* **2015**, *350*, 1222.

[3] J. Byun, H. Cho, C. Wolf, M. Jang, A. Sadhanala, R. H. Friend, H. Yang, T. W. Lee, *Adv. Mater.* **2016**, 7515.

[4] P. Schulz, E. Edri, S. Kirmayer, G. Hodes, D. Cahen, A. Kahn, *Energy Environ. Sci.* **2014**, *7*, 1377.

[5] J. Emara, T. Schnier, N. Pourdavoud, T. Riedl, K. Meerholz, S. Olthof, *Adv. Mater.* **2016**, *28*, 553.

[6] P. Schulz, L. L. Whittaker-Brooks, B. A. Macleod, D. C. Olson, Y. L. Loo, A. Kahn, *Adv. Mater. Interfaces* **2015**, *2*, 1400532.

[7] E. M. Miller, Y. Zhao, C. C. Mercado, S. K. Saha, J. M. Luther, K. Zhu, V. Stevanović, C. L. Perkins, J. van de Lagemaat, *Phys. Chem. Chem. Phys.* **2014**, *16*, 22122.

[8] L. K. Ono, Y. Qi, *J. Phys. Chem. Lett.* **2016**, *7*, 4764.

[9] H. Kawai, G. Giorgi, A. Marini, K. Yamashita, *Nano Lett.* **2015**, *15*, 3103.

[10] J. Endres, D. A. Egger, M. Kulbak, R. A. Kerner, L. Zhao, S. H. Silver, G. Hodes, B. P. Rand, D. Cahen, L. Kronik, A. Kahn, *J. Phys. Chem. Lett.* **2016**, *7*, 2722.

[11] X. Y. Zhu, V. Podzorov, *J. Phys. Chem. Lett.* **2015**, *6*, 4758.

[12] Y. Zhou, G. Long, *J. Phys. Chem. C* **2017**, *121*, 1455.

[13] D. B. Mitzi, K. Chondroudis, C. R. Kagan, *IBM J. Res. Dev.* **2001**, *45*, 29.

[14] D. B. Mitzi, S. Wang, C. A. Feild, C. A. Chess, A. M. Guloy, *Science* **1995**, *267*, 1473.

[15] D. B. Mitzi, C. a. Feild, W. T. a. Harrison, a. M. Guloy, *Nature* **1994**, *369*, 467.

[16] D. B. Mitzi, in *Prog. Inorg. Chem.* (Ed.: K.D. Karlin), John Wiley & Sons, Inc., Hoboken, NJ, USA, **2007**, pp. 1–121.

[17] H. Tsai, W. Nie, J.-C. Blancon, C. C. Stoumpos, R. Asadpour, B. Harutyunyan, A. J. Neukirch, R. Verduzco, J. J. Crochet, S. Tretiak, L. Pedesseau, J. Even, M. A. Alam, G. Gupta, J. Lou, P. M. Ajayan, M. J. Bedzyk, M. G. Kanatzidis, A. D. Mohite, *Nature* **2016**, *536*, 312.

[18] K. Wu, A. Kogo, N. Sakai, M. Ikegami, T. Miyasaka, K., *Chem. Lett.* **2014**, *44*, 321.

[19] L. N. Quan, Y. Zhao, F. P. García De Arquer, R. Sabatini, G. Walters, O. Voznyy, R. Comin, Y. Li, J. Z. Fan, H. Tan, J. Pan, M. Yuan, O. M. Bakr, Z. Lu, D. H. Kim, E. H. Sargent, *Nano Lett.* **2017**, *17*, 3701.

[20] Y. Chen, Y. Sun, J. Peng, W. Zhang, X. Su, K. Zheng, T. Pullerits, Z. Liang, *Adv. Energy Mater.* **2017**, *7*, 1700162.

[21] N. Wang, L. Cheng, R. Ge, S. Zhang, Y. Miao, W. Zou, C. Yi, Y. Sun, Y. Cao, R. Yang, Y. Wei, Q. Guo, Y. Ke, M. Yu, Y. Jin, Y. Liu, Q. Ding, D. Di, L. Yang, G. Xing, H. Tian, C. Jin, F. Gao, R. H. Friend, J. Wang, W. Huang, *Nat. Photonics* **2016**, *10*, 699.

[22] I. B. Koutselas, L. Ducasse, G. C. Papavassiliou, *J. Phys. Condens. Matter* **1999**, *8*, 1217.

[23] K. Tanaka, T. Takahashi, T. Kondo, T. Umebayashi, K. Asai, K. Ema, *Phys. Rev. B - Condens. Matter Mater. Phys.* **2005**, *71*, 1.

[24] T. Ishihara, J. Takahashi, T. Goto, *Phys. Rev. B* **1990**, *42*, 11099.

[25] J. Even, L. Pedesseau, C. Katan, *J. Phys. Chem. C* **2014**, *118*, 11566.

[26] D. H. Cao, C. C. Stoumpos, O. K. Farha, J. T. Hupp, M. G. Kanatzidis, *J. Am. Chem. Soc.* **2015**, *137*, 7843.

[27] M. S. Hybertsen, S. G. Louie, *Phys. Rev. B* **1986**, *34*, 5390.

[28] J. J. Yeh, I. Lindau, *At. data Nucl. data tables* **1985**, *32*, 1.

[29] T. Umebayashi, K. Asai, T. Kondo, A. Nakao, *Phys. Rev. B* **2003**, *67*, 155405.

[30] A. Fox, *Optical Properties of Solids*, Oxford University Press, Oxford, **2010**.

[31] K. Galkowski, A. Mitioglu, A. Miyata, P. Plochocka, O. Portugall, G. E. Eperon, J. T. Wang, T. Stergiopoulos, S. D. Stranks, J. Snaith, R. J. Nicholas, *Energy Environ. Sci.* **2016**, *9*, 962.

[32] A. Mahboubi Soufiani, Z. Yang, T. Young, A. Miyata, A. Surrente, A. Pascoe, K. Galkowski, M. Abdi-Jalebi, R. Brenes, J. Urban, N. Zhang, V. Bulović, O. Portugall, Y.-B. Cheng, R. J. Nicholas, A. Ho-Baillie, M. A. Green, P. Plochocka, S. D. Stranks, *Energy Environ. Sci.* **2017**, *10*, 1358.

[33] J. Feng, B. Xiao, *J. Phys. Chem. Lett.* **2014**, *5*, 1278.

[34] G. Giorgi, J.-I. Fujisawa, H. Segawa, K. Yamashita, *J. Phys. Chem. Lett.* **2013**, *4*, 4213.

[35] C. C. Stoumpos, D. H. Cao, D. J. Clark, J. Young, J. M. Rondinelli, J. I. Jang, J. T. Hupp, M. G. Kanatzidis, *Chem. Mater.* **2016**, *28*, 2852.

[36] P. Umari, E. Mosconi, F. De Angelis, *Sci. Rep.* **2015**, *4*, 4467.

[37] R. Benchamekh, N. A. Gippius, J. Even, M. O. Nestoklon, J. M. Jancu, S. Ithurria, B. Dubertret, A. L. Efros, P. Voisin, *Phys. Rev. B - Condens. Matter Mater. Phys.* **2014**, *89*, 35307.

[38] K. Tanaka, T. Takahashi, T. Kondo, K. Umeda, K. Ema, T. Umebayashi, K. Asai, K. Uchida, N. Miura, *Japanese J. Appl. Physics, Part 1 Regul. Pap. Short Notes Rev. Pap.* **2005**, *44*, 5923.

[39] O. Yaffe, A. Chernikov, Z. M. Norman, Y. Zhong, A. Velauthapillai, A. van der Zande, J. S. Owen, T. F. Heinz, *Phys. Rev. B* **2015**, *92*, 45414.

[40] J.-C.-C. Blancon, H. Tsai, W. Nie, C. C. Stoumpos, L. Pedesseau, C. Katan, M. Kepenekian, C. M. M. Soe, K. Appavoo, M. Y. Sfeir, S. Tretiak, P. M. Ajayan, M. G. Kanatzidis, J. Even, J. J. Crochet, A. D. Mohite, *Science* **2017**, *355*, 1.

[41] D. Niesner, M. Wilhelm, I. Levchuk, A. Osvet, S. Shrestha, M. Batentschuk, C. Brabec, T. Fauster, *Phys. Rev. Lett.* **2016**, *117*, 14701.

[42] K. Gauthron, J.-S. Lauret, L. Doyennette, G. Lanty, A. Al Choueiry, S. J. Zhang, A. Brehier, L. Largeau, O. Mauguin, J. Bloch, E. Deleporte, *Opt. Express* **2010**, *18*, 5912.

[43] A. Miyata, A. Mitioglu, P. Plochocka, O. Portugall, J. T.-W. Wang, S. D. Stranks, H. J. Snaith, R. J. Nicholas, *Nat. Phys.* **2015**, *11*, 582.

[44] C. F. Klingshirn, *Semiconductor Optics*, Springer, Berlin, **2012**.

[45] A. Schindlmayr, *Eur. J. Phys.* **1997**, *18*, 374.

[46] R. de L. Kronig, W. G. Penney, *Proc. R. Soc. A Math. Phys. Eng. Sci.* **1931**, *130*, 499.

[47] G. Bastard, *Phys. Rev. B* **1981**, *24*, 5693.

[48] H. S. Cho, P. R. Prucnal, *Phys. Rev. B* **1987**, *36*, 3237.

[49] P. F. Yuh, K. L. Wang, *Phys. Rev. B* **1988**, *38*, 13307.

[50] E. Menéndez-Proupin, P. Palacios, P. Wahnón, J. C. Conesa, *Phys. Rev. B* **2014**, *90*, 45207.

[51] C. I. Wu, Y. Hirose, H. Sirringhaus, A. Kahn, *Chem. Phys. Lett.* **1997**, *272*, 43.

[52] G. Kresse, D. Joubert, *Phys. Rev. B* **1999**, *59*, 1758.

[53] G. Kresse, J. Furthmüller, *Comput. Mater. Sci.* **1996**, *6*, 15.

[54] L. Dou, A. B. Wong, Y. Yu, M. Lai, N. Kornienko, N. S. Ginsberg, L. Wang, A. P. Alivisatos, P. Yang, *Science* **2015**, *349*, 1518.

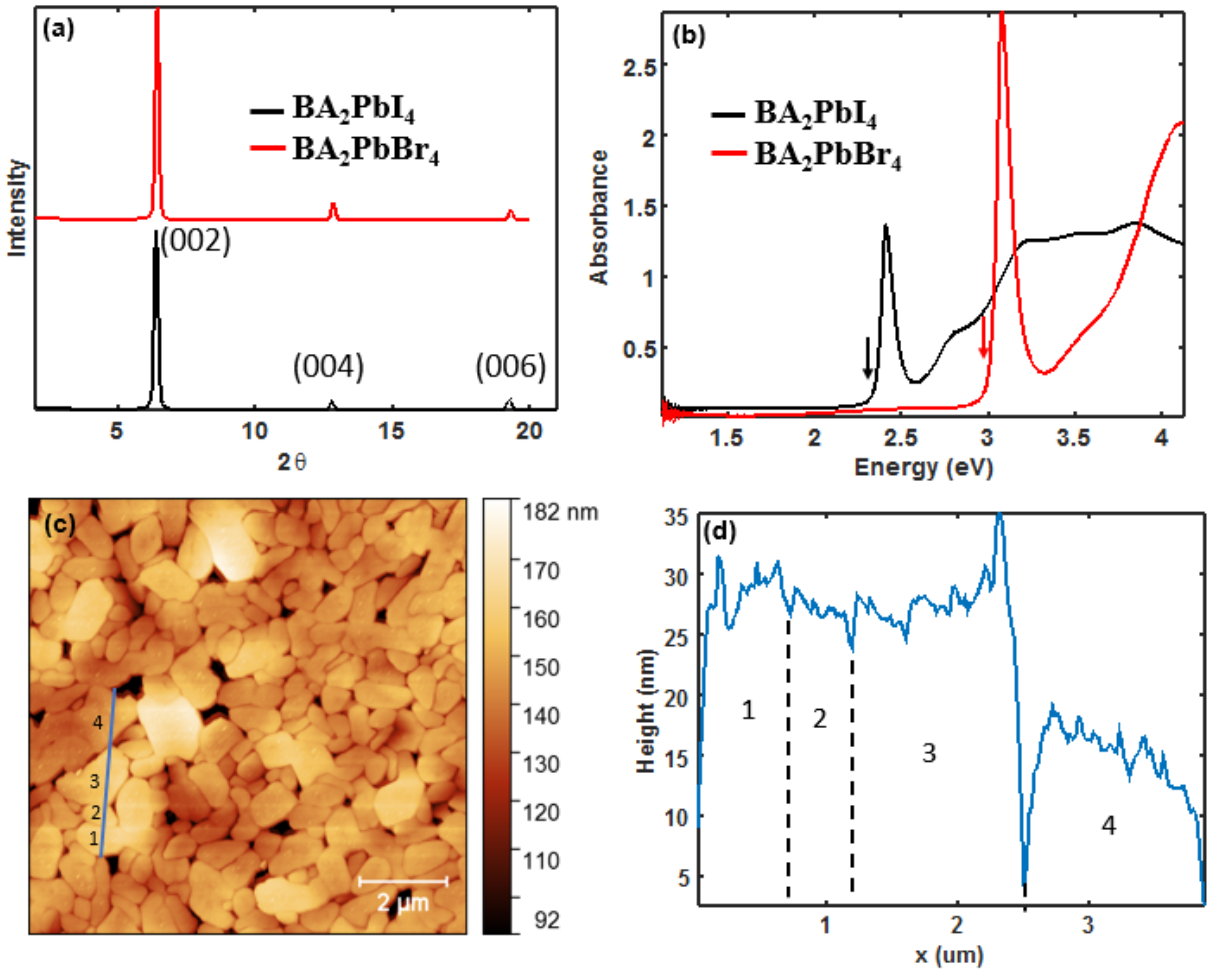

Figure 1. (a) XRD spectra of BA2PbI4 and BA2PbBr4 thin films showing well-oriented, phase-pure films. (b) Optical absorption spectra of both films on glass, each showing a distinct excitonic peak followed by the onset of band-to-band absorption (c) AFM image of the microstructure of the spin-coated BA2PbI4 thin film. A line profile of the grains labeled 1-4 can be seen in figure (d).

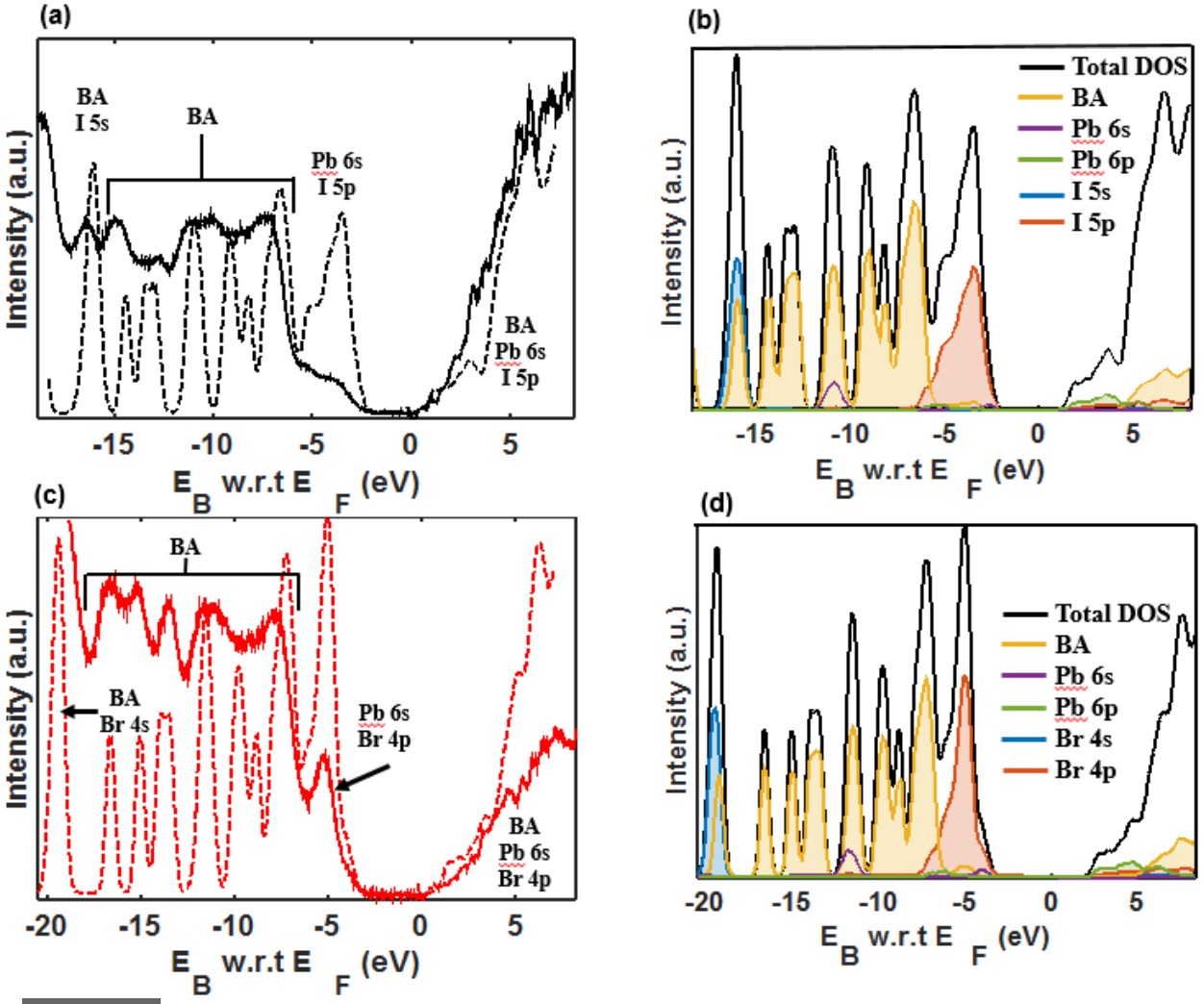

Figure 2. (a) The DOS of BA2PbI4 as determined by UPS (He-II) and IPES experiments and DFT carried out at the HSE+SOC level as solid and dashed lines, respectively. The DFT DOS was stretched 10% and shifted to match the features of the experimental DOS. The data are plotted with respect to the Fermi level. (b) The DOS of BA2PbI4 determined at the HSE+SOC level of theory divided into its molecular and atomic orbital contributions. The same for BA2PbBr4 is shown in (c), (d). The calculated DOS with a Gaussian smearing of 0.05 is shown in Figure S1

.

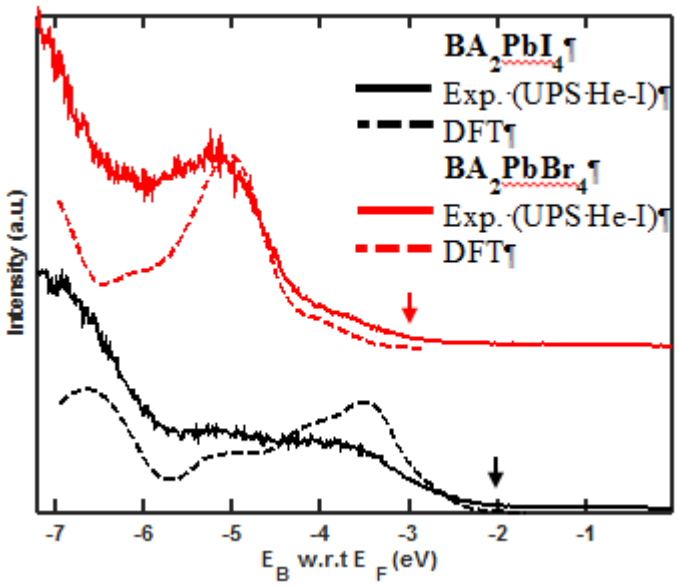

Figure 3. UPS (He-I) spectra of a close-up of the DOS in the valence band of BA2PbI4 and BA2PbBr4 in solid lines compared with DFT carried out at the HSE+SOC level in dashed lines. The data is plotted with respect to the Fermi level.

Table I. Calculated hole and electron effective mass ($\times m_0$) along Γ-X of BA_2PbBr_4 and BA_2PbI_4 with and without SOC effects at the GGA/PBE level.

Compounds	m_{hole} [m_0]		$m_{electron}$ (m_0]	
	Γ-X (without SOC)	Γ-X (with SOC)	Γ-X (without SOC)	Γ-X (with SOC)
BA_2PbI_4	0.111	0.111	0.098	0.087
BA_2PbBr_4	0.112	0.090	0.088	0.071

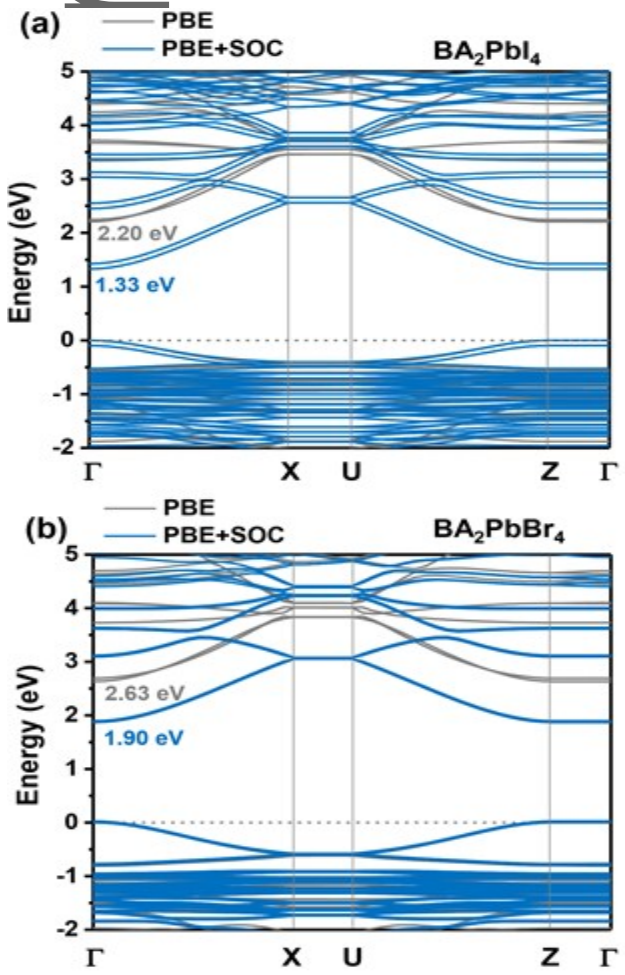

Figure 4. Band structures with and without account of SOC effects, as calculated at the GGA/PBE level for (a) BA_2PbI_4 and (b) BA_2PbBr_4.

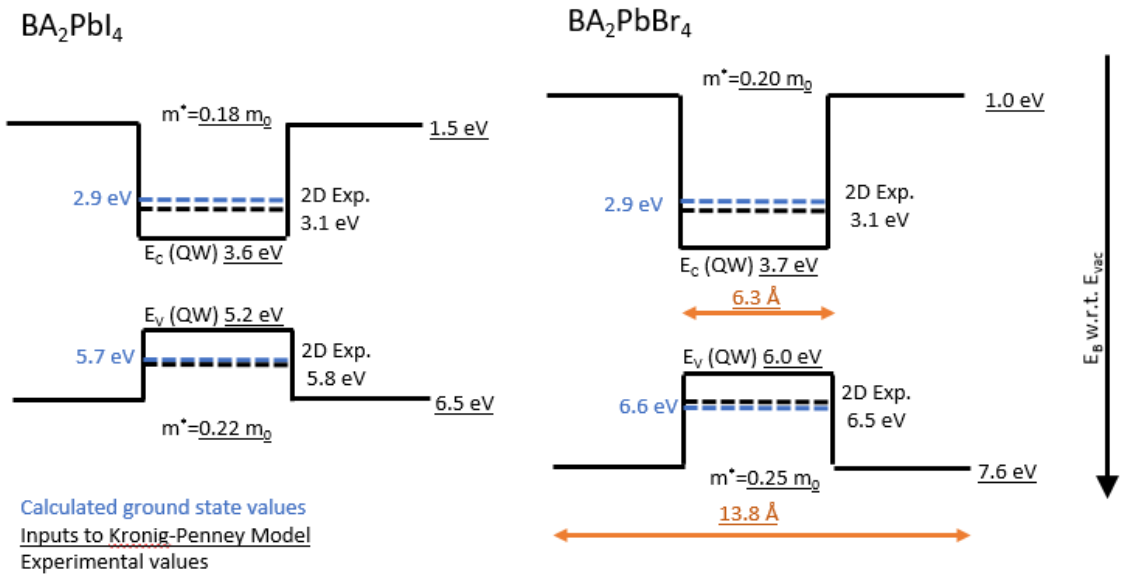

Figure 5. Diagram of the quantum wells formed in BA2PbI4 and BA2PbBr4. The values for EC(QW) and EV(QW) are taken from Endres et al.[9] The heights of the conduction and valence band wells are defined in the text. The blue dashed line represents the calculated value of the quantum well state based on the barrier height, well width and effective mass. The black dashed line represents the experimentally determined band edges of BA2PbI4 and BA2PbBr4.

Table of Contents:

Understanding the density of electronic states (DOS) in two-dimensional metal halide perovskites is a crucial step in the investigation of the fundamental properties of these materials. This combined experimental - theoretical study via direct and inverse photoemission spectroscopy and density functional theory calculations maps out the various contributions from organic and inorganic constituents to the DOS of the materials.

Keywords: perovskites, two-dimensional materials, quantum wells, photoelectron spectroscopy, DFT calculations

Scott Silver, Jun Yin, Hong Li, Jean-Luc Brédas, Antoine Kahn*

Characterization of the Valence and Conduction Band Levels of n=1 Two-Dimensional Perovskites: A Combined Experimental and Theoretical Investigation